

# MAPPING LONG-TERM STABILITY REGIONS USING THE FAST LYAPUNOV INDICATOR

Benjamin F. Villac<sup>\*</sup>; John J. Aiello<sup>†</sup>

The determination and characterization of long-term stability regions around periodic orbits (i.e. small, bounded variations in the action elements of a spacecraft for several hundred to a thousand years) is addressed using a modern numerical tool for the detection of chaotic motion: the Fast Lyapunov Indicator (FLI). Long-term stability regions are important for spacecraft applications as they can be used as disposal regions for end of mission requirements. The method is applied to the case of distant retrograde orbits around the Jupiter's moon Europa. It is shown that the extent of the stability region decreases with the stability index of the periodic orbit family, reducing to an empty set in a neighborhood of the colinear libration point regions.

## INTRODUCTION

Planetary protection requirements often preclude the impact of a spacecraft on a celestial body that may shelter life. The disposal of the spacecraft at the end of the mission becomes one of the challenges that a mission trajectory designer must face. Aside from the minimization of the amount of fuel required for this last transfer (which thus enters into the global budget of the mission), this problem involves the additional constraint of avoiding impact with the given celestial body, and possibly other, for a conventional, and ideally very long, amount of time (e.g. several hundred years).

In the case of a Jupiter orbiter, Friedlander<sup>3</sup> estimated probabilities of impact with the different moons of Jupiter over a period of 50 years. His study used a statistical approach over a limited range of trajectories that would supposedly correspond to end of mission trajectories of a Jupiter orbiter. These results show that the risk of impact of a spacecraft with one of the Galilean moons of Jupiter over a period of 50 years is very high for trajectories crossing the paths of the moons. While these results

---

<sup>\*</sup>Staff Engineer, Jet Propulsion Laboratory, California Institute of Technology, 4800 Oak Grove Drive, Pasadena, CA 91101. E-mail: Benjamin.F.Villac@jpl.nasa.gov.

<sup>†</sup>Senior Engineer, Jet Propulsion Laboratory, California Institute of Technology, 4800 Oak Grove Drive, Pasadena, CA 91109.

are useful for gaining some insights into the impact risk problem, they do not provide the mission designer with a definite method to locate and to estimate the size of the stability regions.

Indeed, for unusually long time spans, direct numerical integration of large sets of trajectories can become prohibitively time-consuming, while stability over short time spans does not indicate a priori the long term behavior of the stable orbits computed. By using our knowledge of the dynamical structure of the systems considered, the integration of trajectories over relatively short time spans can be used to produce long term stability prediction. For example, results from modern perturbation theory introduced a distinction between regular or quasi-periodic trajectories and chaotic motion<sup>13</sup> and indicate that regions of phase space densely filled with regular trajectories present the desired long term stability. As celestial mechanics have observed during the last few decades, quasi-periodic trajectories and chaotic motion have very different properties that can be analyzed numerically. Chaoticity indicators are used for these purposes. For example, the well-known Lyapunov exponent, which characterizes divergence of nearby trajectories, can be used as such an indicator, as it reduces to zero for regular motion and takes a strictly positive value for chaotic motion<sup>13,14</sup>. While the computation of the Maximal Lyapunov Exponent (MLE) requires the estimation of a limit, it has been shown that the computation of such an exponent for a limited time is generally sufficient to discriminate between regular and chaotic motion. Such an estimation is referred to as the Fast Lyapunov Indicator or FLI<sup>4,5</sup>.

After reviewing some results in modern perturbation theory in order to clarify the notion of stability, this paper investigates the use of the FLI to compute the extent of the stability domains that exist around stable periodic orbits, for example. The method is applied to the family of Distant Retrograde Orbits (DRO) that exist around planetary satellites as a continuation of the equatorial, retrograde, circular orbits of a central force problem into a restricted three-body model<sup>9</sup>.

## THEORETICAL BACKGROUND

When the Keplerian energy is negative, relative motion of neighboring particles in a two body problem can lead to secular drifts in the along-track direction. The local qualitative features of these dynamics are well represented by the Clohessy-Wiltshire equations. Thus, the two body problem is unstable from a state space control viewpoint. However, when considering spacecraft disposal orbits, one is not generally concerned with the relative motion with respect to a nominal trajectory but is more likely interested in the relative motion with respect to a nominal *orbit*. The distinction between trajectory (time evolution of the motion) and orbit (geometric path described by the particle) can be understood in terms of orbital elements, namely: stability occurs when no secular drift in quantities such as semi-major axis,  $a$ , eccentricity,  $e$ , and inclination,  $i$ , ( $\sim$  action variables) occur, while any drift in longitude

of the ascending node,  $\Omega$ , the argument of periapsis,  $\omega$  and the mean anomaly,  $M$ , ( $\sim$  angle variables) are of no importance. In this framework, the two-body problem is stable around any given nominal orbit when the energy is negative.

In order to clarify the terminology and rationale of the method to be presented in the next section, we review here the modern dynamical theoretical background to analyze this “secular stability”. References for this material can be found in the original research articles<sup>1</sup> or textbooks<sup>13</sup>.

## Integrable Systems and Invariant Tori

In order to introduce some definitions we consider the dynamics in the planar two-body problem, when viewed in a rotating frame (PR2BP). This is one of the basic integrable systems that appears in astrodynamics and corresponds to the unperturbed dynamics of the systems considered in this paper.

Denoting  $(x, y)$  as the Cartesian coordinates in the rotating frame, the equations of motion of this dynamical system are given by:

$$\begin{cases} \ddot{x} - 2\dot{y} - x &= -\frac{x}{r^3} \\ \ddot{y} + 2\dot{x} - y &= -\frac{y}{r^3} \end{cases}$$

where  $r = \sqrt{x^2 + y^2}$  and the angular velocity of the frame and gravitational parameter of the central body have been normalized to one.

The Hamiltonian of the system is given by:

$$\mathcal{H}_0 = \frac{1}{2} \{ (p_x + y)^2 + (p_y - x)^2 \} + \frac{1}{2} (x^2 + y^2) - \frac{1}{r}$$

where  $p_x = \dot{x} - y$  and  $p_y = \dot{y} + x$  represent the momenta associated with the coordinates  $x$  and  $y$ . Another useful formulation is obtained when using the Delaunay elements<sup>13</sup>, which correspond to a set of action-angle variables for the problem.

$$\mathcal{H}_0 = -\frac{1}{2L^2} + G \tag{1}$$

where  $L = \sqrt{a}$  and  $G = \sqrt{a(1 - e^2)}$  correspond to the actions, the conjugate angle variables being  $M$  and  $\tilde{\omega}$ , the longitude of periapsis defined with respect the the rotating  $x$ -axis.

*Invariant Tori.* While all the trajectories are simply periodic in inertial space, this is not the case in the rotating frame where both periodic and quasi-periodic motion coexist. From the Hamiltonian (1) and Hamilton’s equations, we easily see that each trajectory is determined by a set of fixed values of  $(a, e)$  and a linear time variation

in the longitude of the periapsis,  $\tilde{\omega} = -t$ , and the mean anomaly,  $M = nt$ , where  $n = a^{-3/2}$  represents the mean motion. Geometrically, at fixed values of  $(a, e)$ , the space of all the possible values of  $(\Omega, \omega)$  form a 2-dimensional torus. Since the time evolution of a trajectory starting on a given torus stays on the same torus for all times, these tori are called *invariant tori*.

As time varies, any initial condition  $(\Omega_0, M_0)$  will result in a line wrapping on an invariant torus and two main cases can be distinguished:

- When  $M/\tilde{\omega}$  is rational\*, say  $r/s$ , then the motion is *periodic* with period  $2\pi s$ . Each period corresponds to  $r$  revolutions in mean anomaly and  $s$  revolutions in longitude of the periapsis. Each initial condition on the same torus will lead to periodic motion with the same characteristics (e.g. period), thus foliating the  $2D$ -torus in invariant  $1D$ -tori (i.e. the periodic orbits). The torus for which such a foliation occurs are called *resonant tori*. Note that the property of being resonant depends only on the values of the action variables, here  $a$  and  $e$ , and not on the angles. Indeed, the condition  $M/\tilde{\omega} = r/s$  can be reformulated as  $sn + r = 0$ , where  $n = a^{-3/2} = L^{-3}$  is the mean motion.

More generally we will say that an initial condition  $(\mathbf{I}, \boldsymbol{\phi})$  of an integrable system  $\mathcal{H}(\mathbf{I})$ , where  $(\mathbf{I}, \boldsymbol{\phi})$  are action-angle variables, is resonant if there exists a non-zero vector,  $\mathbf{k}$ , with integer entries such that the dot product between the frequencies  $\boldsymbol{\omega} = \partial\mathcal{H}/\partial\mathbf{I}$  and  $\mathbf{k}$  is zero:

$$\exists \mathbf{k} \in \mathbb{Z}^n, \mathbf{k} \neq 0 \quad \text{such that} \quad k_1 \omega_1(\mathbf{I}) + \dots + k_n \omega_n(\mathbf{I}) = 0$$

- When  $M/\tilde{\omega}$  is irrational the trajectory never closes upon itself and densely fills the invariant  $2D$ -tori. Given any values of  $\tilde{\omega}$  and  $M$  on the torus, the trajectory will eventually reach any neighborhood of this point at some point in time. Such tori are called *non-resonant* and the trajectories lying on it are called *quasi-periodic*.

In the general setting, a non-resonant tori is characterized by action variables such that:

$$\forall \mathbf{k} \in \mathbb{Z}^n, \mathbf{k} \neq 0 \quad \text{we have} \quad k_1 \omega_1(\mathbf{I}) + \dots + k_n \omega_n(\mathbf{I}) \neq 0$$

We will say, moreover, that the non-resonant torus is diophantine if the frequencies satisfy the following condition with some constant  $\gamma > 0$  and  $\tau > n - 1$ :

$$|\mathbf{k} \cdot \boldsymbol{\omega}(\mathbf{I})| > \frac{\gamma}{|\mathbf{k}|^\tau}, \quad \forall \mathbf{k} \in \mathbb{Z}^n, \mathbf{k} \neq 0$$

---

\*In the model problem considered, the fact of being rational (resonant) or non-rational (non-resonant) depends only on the semi-major axis,  $a$ , since  $n = a^{-3/2}$  only depends on  $a$  while the frequency corresponding to the longitude of the periapsis is independent of both  $a$  and  $e$ .

When using the Cartesian coordinates  $(x, y)$ , the tori will appear as distorted “donut” surfaces formed by families of periodic orbits in the resonant case, and a set of quasi-periodic orbits in the non-resonant case<sup>†</sup>. Figure 1 illustrates those classic dynamical phenomena in the  $(x, y, \dot{x})$  space. Motion lying on such invariant tori will be called *perpetually stable*.

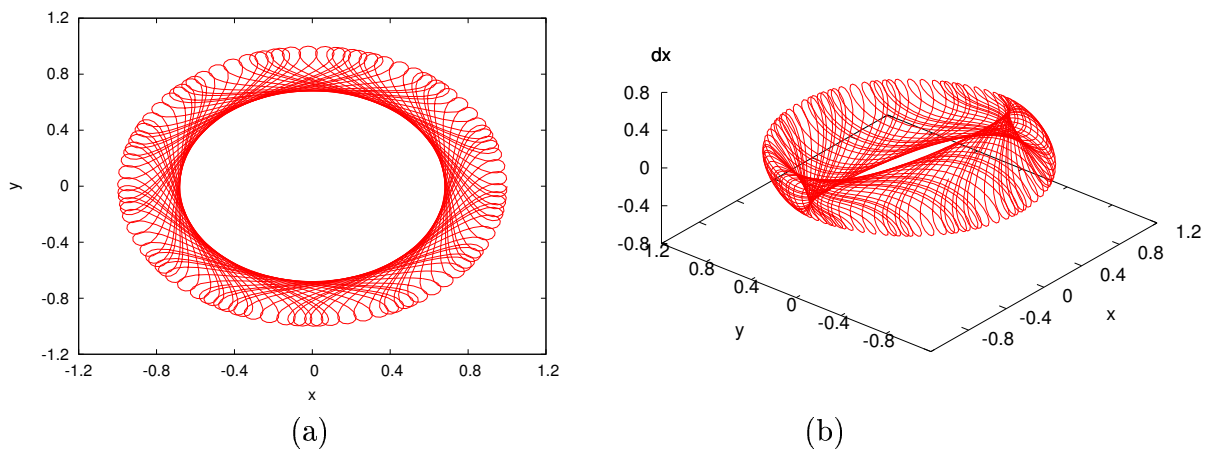


**Figure 1: Sample quasi-periodic trajectory in the PR2BP integrated for 500 units of time. (a) projection in configuration space. (b) 3D representation of the invariant torus associated with the trajectory.**

*Poincaré maps.* In order to succinctly represent a family of invariant tori in a 2 degree of freedom system, the concept of a *Poincaré map*, which consists of associating each trajectory with its sequence of successive crossings with a surface of section (of codimension 1) in phase space, can be used. It is generally assumed that an energy integral exists and that the Poincaré map is further reduced to an energy manifold so that the surface of section restricted to the energy manifold is now 2 dimensional. The definition of a Poincaré map may only be local and is well defined only on the domain of transversality of the flow with respect to this surface of section.

For example, in the above planar two-body problem one can define the surface of section as the plane  $y = 0$ , considering crossings for which  $\dot{y} > 0$ , so that each such crossing is fully represented by the values of  $(x, \dot{x})$  at a fixed “Jacobi” energy  $C = -2\mathcal{H}$ . Figure 2(a) presents the result of the computation of such a map.

As we can see, the iterates of a quasi-periodic trajectory form a closed curve that represents the section of the  $2D$  invariant tori on which it lies. Periodic orbits are

---

<sup>†</sup>Only one quasi-periodic trajectory is necessary to obtain an idea on the shape of the invariant tori since any such trajectory will densely fill this tori.

represented as a discrete sequence of points. Thus the representation of a Poincaré map allows us to represent a whole slice of the dynamics and easily recognize the invariant tori in the  $2D$  case.

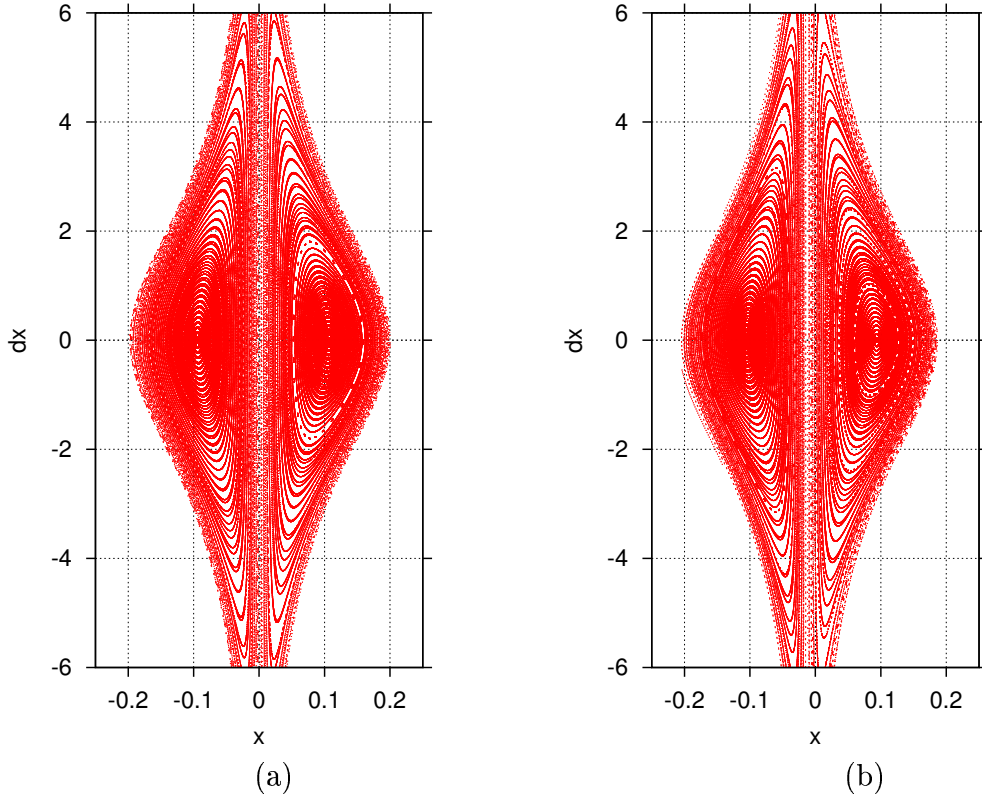


**Figure 2: Sample Poincaré maps: (a) PR2BP,  $C = 10.0$ ; (b) PCR3BP,  $\mu = 0.012$ ,  $C = 10.0$ .**

## Non-integrable Systems and Stability Issues

The two-body problem is, of course, an idealized problem and one can wonder what happens to these dynamics, and especially to the stability properties of trajectories, when perturbations are introduced. For example, the Planar Circular Restricted 3-Body Problem (PCR3BP), a classical model<sup>17</sup> used in astrodynamical studies and preliminary mission trajectory design<sup>7</sup>, can be viewed as a perturbed two-body problem in a rotating frame, where the perturbation models the introduction of a third body. This model will be used in the following discussion for purpose of illustration, as well as for its own astrodynamical interest.

The convention adopted for the PCR3BP will be that of a barycentric rotating frame with angular velocity normalized to one, the most massive body,  $M_1$ , of mass  $\nu = 1 - \mu$  lying on the negative  $x$ -axis at  $-\mu$ , while the other primary,  $M_2$ , of mass  $\mu$  will also be located on the  $x$ -axis at  $\nu$ . In this setting, the equations of motion are

given by the Hamiltonian  $\mathcal{H}$ :

$$\mathcal{H} = \frac{1}{2} \{ (p_x + y)^2 + (p_y - x)^2 \} + \frac{1}{2} (x^2 + y^2) - \frac{\nu}{r_1} - \frac{\mu}{r_2} \quad (2)$$

where  $r_1 = \sqrt{(x + \mu)^2 + y^2}$  is the distance from the spacecraft to  $M_1$ , while  $r_2 = \sqrt{(x - \nu)^2 + y^2}$  is the distance from  $M_2$ . The quantity  $C = -2\mathcal{H} = 2\Omega(x, y) - v^2$ , will be referred as the Jacobi constant and represents a first integral of the motion ( $v = \sqrt{\dot{x}^2 + \dot{y}^2}$  being the speed of the spacecraft).

*Small perturbations and nearly-integrable systems.* When the added perturbations are small and conservative, the dynamical system can be modeled by a Hamiltonian of the form:

$$\mathcal{H}(\mathbf{I}, \boldsymbol{\phi}) = \mathcal{H}_0(\mathbf{I}) + \epsilon \mathcal{H}_1(\mathbf{I}, \boldsymbol{\phi}) \quad (3)$$

where  $(\mathbf{I}, \boldsymbol{\phi})$  represents action-angle variables,  $\mathcal{H}_0$  is assumed to be integrable,  $\mathcal{H}_1$  to be analytic and of the same order as  $\mathcal{H}_0$  and  $\epsilon \ll 1$ . Kolmogorov, Arnold and Moser (KAM) proved a series of results that allow us to conclude<sup>‡</sup> that for small enough conservative perturbations the majority of the invariant *diophantine* tori of  $\mathcal{H}_0$  do persist in the perturbed system,  $\mathcal{H}$ , thus showing the existence of perpetually stable motion in such systems. Moreover, it can be shown that the action variables vary periodically with respect to the angle variables.

For example, performing the change of variables  $x \rightarrow x + \mu$  or  $x \rightarrow x + \nu$ , the PCR3BP can be cast into the form (3) for large enough values of  $C$ . Since the PR2BP is iso-energetically non-degenerate, KAM theory predicts that most invariant tori of the rotating two body problem are still present in the PCR3BP. This can be heuristically checked by computing a Poincaré map, as shown in Figure 2(b).

While the notion of perpetual stability is certainly of interest and will be the backbone of the numerical method to be used in the next section, the set of perpetually stable trajectories has a complex structure that does not reflect the physical notion of a stability region. Indeed, the resonant tori are not generally preserved and leave the place to regions in phase space with complex dynamics, mixing chaotic motion with islands of regular motion. Chaotic motion, associated with the presence of unstable periodic orbits, homoclinic and heteroclinic points, is characterized by a continuous spectrum of the action variables that results in a random-like behavior of chaotic trajectories. On the contrary, resonant islands, associated with stable periodic orbits, are regions densely filled with invariant tori; KAM theory being in fact applicable in these regions after a normalization process in the resonance region<sup>13</sup>. While in 2D systems the existence of chaotic layers does not prevent the system from being globally, perpetually stable, this is not so for the 3 degree of freedom systems, where diffusion of the action variables along resonances can occur.

This lack of regions densely filled with invariant tori to form a continuous, open

---

<sup>‡</sup>Assuming some degeneracy condition on  $\mathcal{H}_0$ .

domain in phase space is alleviated by several results which, for small enough perturbations, indicate that the diffusion time of the chaotic trajectories initially in a neighborhood of a KAM torus is exponentially long<sup>15,13</sup> (effective stability). The foundational result of this subject, the Nekoroshev theorem, states that under non-degeneracy and convexity assumptions on  $\mathcal{H}_0$ , the variation of the actions under the flow of the Hamiltonian (3), satisfies the following relations:

$$\forall \epsilon < \bar{\epsilon}, \quad \forall t \leq T(\epsilon) = c_1 \sqrt{\frac{\bar{\epsilon}}{\epsilon}} \exp\left(\frac{\bar{\epsilon}}{\epsilon}\right)^{c_2}, \quad \|\mathbf{I}(t) - \mathbf{I}_0\| \leq c_3 \epsilon^{c_4} \quad (4)$$

for suitable positive constant  $c_i$  and  $\bar{\epsilon}$  and any initial condition  $\mathbf{I}_0$  in a given open neighborhood of phase space. Thus, a trajectory can be said to be effectively stable when its action variables satisfy the above relations and the set of such trajectories can be taken as the definition of a stability region.

Thus, stability regions form open domains of phase space that contain the preserved KAM tori<sup>§</sup>. In fact, as the diffusion time  $T(\epsilon)$  gets larger when closer to a KAM torus<sup>15</sup>, regions packed with invariant KAM tori correspond to effectively stable regions. Thus, this notion of effective stability gives substance to our physical notion of a stability region.

*Large perturbations and physical systems.* The above discussion would a priori seem useless for our purpose as the hypothesis of small perturbations is far from being satisfied in spacecraft applications and the above theories requires an Hamiltonian of the form introduced by equation (3) with a small  $\epsilon$ . For example, the transit dynamics of a spacecraft through the libration point regions is the result of a 1 : 1 resonance with the primaries. Figure 3 presents a Poincaré section of the PCR3BP obtained at larger values of energy, showing the predominance of chaotic motion.

As we briefly mentioned however, all the above stability theories are applicable locally if, after some normalization process, the dynamics can be cast into the required nearly-integrable form as given by equation (3). For instance, we have seen that the above theories were applicable to the PCR3BP where the small parameter condition can be translated as a condition on the value of  $C$ . While this case is not of interest for spacecraft applications, the dynamics around a stable periodic orbit is. For example, Figure 4 presents a Poincaré map around a Distant Retrograde Orbit (DRO)<sup>9</sup> showing a structure of densely filled invariant tori surrounded by a large chaotic sea. The above theory is applicable to that case around the center of the resonant island filled by the invariant tori. The small parameter could be taken in that case as the distance from the nominal DRO.

In summary, the above results indicate that regions densely packed with regular trajectories correspond to regions of *very* long term stability and should represent ideal regions of phase space for very long term spacecraft disposal orbits.

---

<sup>§</sup>Since in that case,  $T(\epsilon) = +\infty$ .

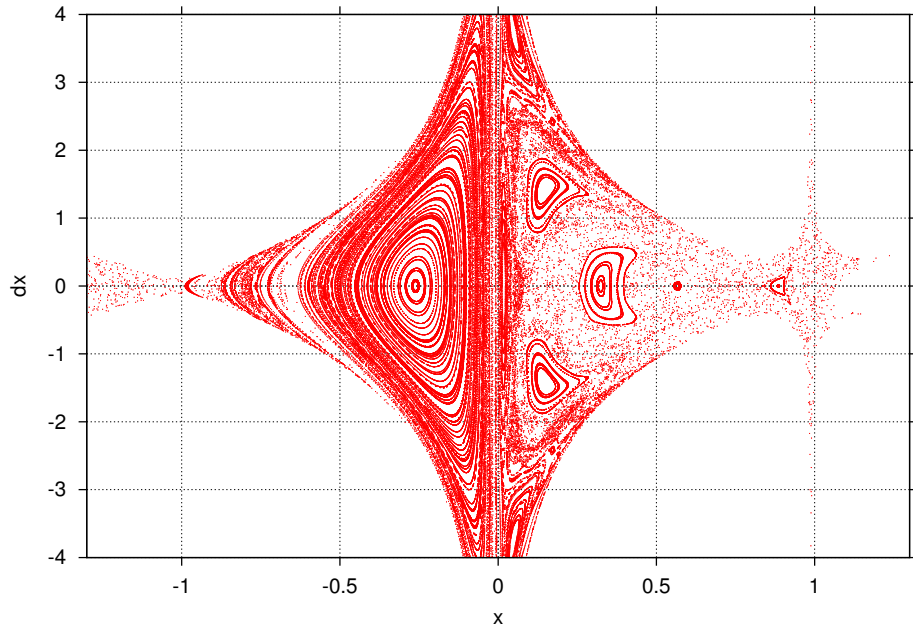


**Figure 3:** Poincaré map in the PCR3BP for the Earth-Moon system ( $\mu = 0.012$ ) at  $C = 3.0$ . As we can see, large region of phase space are dominated by chaotic motion.

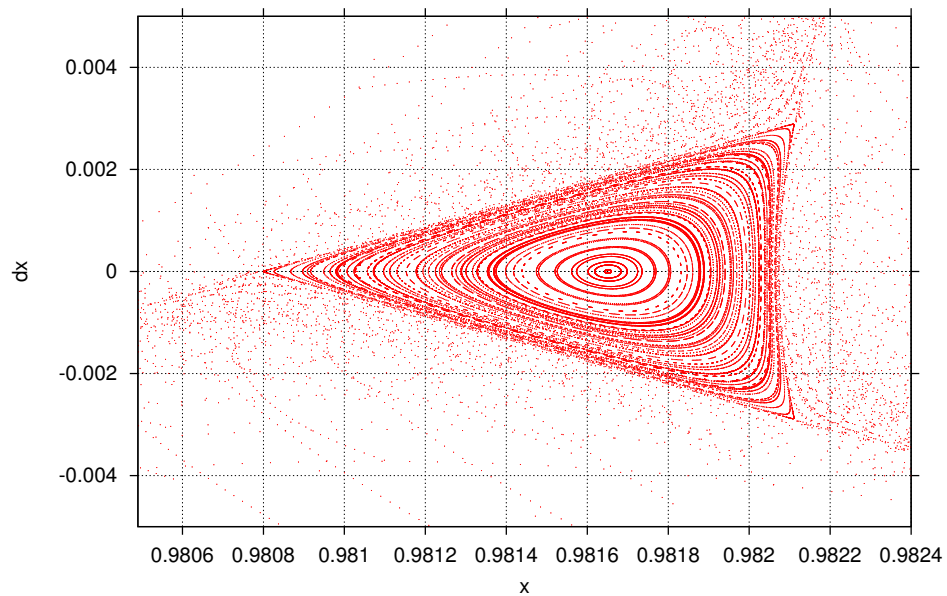


**Figure 4:** Poincaré map in the PCR3BP near a stable periodic orbit for  $C = 3.0$  in the Europa-Jupiter system ( $\mu = 2.528 \times 10^{-5}$ ).

## STABILITY REGIONS COMPUTATION

To analyze a property  $P$  of a set of trajectories over a given time span one can sample a fixed region of initial conditions and compute the property of each initial condition over the given time span, thus generating a contour map (or density plot) of the property over the set of initial conditions considered (“ $P$  map”). For example, in order to test the stability properties of a region of phase space one can a priori integrate the set of trajectories for the desired length of time and determine if the variation of the action variables remains bounded over that given time span<sup>¶</sup>. While this method is perfectly valid for relatively short time spans, the computational efforts quickly become prohibitive as the length of time is increased. The theoretical background presented in the previous section allows us, however, to significantly mitigate this computational effort by generating long term stability maps while using relatively short integration time. Indeed, we have seen that the stability regions considered correspond to the effective stability regions which can be approximated by the set of regular trajectories. This last property can be determined numerically by using chaoticity indicators, some of which require only limited computational effort.

### Chaoticity Indicators

Chaoticity indicators provide a means of distinguishing between chaotic and regular motion. The first indicator appeared in the work of Lyapunov<sup>12</sup> and Oseledec<sup>14</sup> and is now generally referred to as the Maximum Lyapunov Exponent (MLE),  $\gamma$ .

$$\gamma = \lim_{t \rightarrow \infty} \frac{\ln \|v(t)\|}{t}$$

where  $v(t)$  is the image of an initial tangent vector to the phase space at the initial condition considered by the state transition matrix. That is,  $v(t)$  is obtained by integrating the system of first variational equations.

This indicator can be shown to be zero for any kind of regular motion (i.e. resonant or not), while it does take a strictly positive value for a chaotic trajectory. While the MLE has sound theoretical basis its numerical evaluation requires very lengthy integration time span to ascertain for the convergence of the limit and is thus not well suited for our purpose.

Froeschlé et al.<sup>4</sup> investigated the behavior of the tangent vector  $v(t)$  for shorter time spans and showed the possibility of distinguishing chaotic trajectories from regular ones with a much smaller integration time than that required for the MLE. These authors called this indicator the Fast Lyapunov Indicator, or FLI for short. This indicator has been shown to be very sensitive while requiring much less computational

---

<sup>¶</sup>or check for some other criteria admissible for the chosen definition of stability, such as the existence or not of an impact event with another celestial body.

effort than other chaoticity indicators. This is the indicator that we will use for the subsequent investigations.

For completeness, we mention that many other chaoticity indicators are available. They can be classified into two main groups according to their use of the properties of the tangent mapping to the flow, i.e. the state transition matrix (e.g. the FLI and MLE are part of this group), or their use of the frequency differences between regular and chaotic trajectories (e.g., the Frequency Analysis Map or FAM<sup>10</sup>).

## The Fast Lyapunov Indicator

Several definitions of the FLI can be found in the literature. In reference (Ref. 4), Froeschle et al. investigated the behavior of the following function of the tangent vectors,  $\psi_1, \dots, \psi_3$ , while they used the function  $\psi_4$  in reference (Ref. 5):

$$\psi_1 = \frac{1}{\|v_1(t)\|^n} \quad ; \quad \psi_2 = \frac{1}{\prod_{j=1,n} \|v_j(t)\|} \quad ; \quad \psi_3 = \frac{1}{\sup_j \|v_j(t)\|^n} \quad ; \quad \psi_4 = \sup_{t \leq \tau} \ln \|v(t)\|$$

where  $(v_i)$  is a basis of tangent vectors, and  $v(t)$  is an arbitrary tangent vector.

The differences between these definitions lie in their sensitivity to the choice of the initial vector (basis) and their ability to distinguish between resonant and non-resonant regular motion. The choice of  $\psi_3$  for example reduces the dependence with respect to the initial basis while the choice of a single vector allows the distinction between resonant and non-resonant regular motion. The definition of  $\psi_4$  is also closer to the definition of the MLE and the scaling used seems to have the right scaling to accentuate quickly the difference between regular and chaotic motion.

For our purposes the distinction between resonant island and non-resonant regular motion is not as important as the independence with respect to the initial basis, and a merging of the definitions of  $\psi_3$  and  $\psi_4$  has been used to obtain an indicator as close as possible to the definition of the MLE while requiring much less time to discriminate between regular and chaotic motion and depending as little as possible on the choice of the initial vector basis:

$$\psi = \sup_{\tau \leq t} \sup_i \ln \|v_i(\tau)\|$$

Note that this definition is rather arbitrary<sup>||</sup> but what really matters is the strong difference of behavior of this indicator for regular and chaotic motion, as we illustrate

---

<sup>||</sup>While the independence with respect to the choice of basis vector is weaker than for a single vector, it is still dependent on it. Also, the choice of the norm used influences the exact value of  $\phi$  obtained at any given time. In this paper the standard basis of vectors and the Euclidean norm have been used.

below. In the following discussion, we will call FLI the value of  $\psi$  at a given instant in time.

From the results of the Lyapunov exponents theory we can see that  $\psi$  should increase faster for chaotic rather than regular trajectories so that, given a fixed integration time  $T$ , the chaotic trajectories will be characterized by a high value of  $\psi$  as compared to the regular ones. This argument is however heuristic since the MLE is defined as a limit which can require a very long integration time before showing its behavior. A more rigorous argument has been given in reference (Ref. 8).

Figure 5(a) presents the FLI variation with time of two different trajectories with initial conditions taken on the Poincaré section first presented in Figure 4. The first trajectory considered is regular and corresponds to the periodic orbit at the center of the stability region while the second trajectory corresponds to a chaotic one, taken at an arbitrary point in the chaotic sea. As we can observe from Figure 5, the FLI value of the chaotic trajectory grows much faster than for the regular one. In our case, after a time difference of  $T = 400$ , the jump in the FLI value is about 27, which corresponds to a relative difference\*\* of more than 300%.

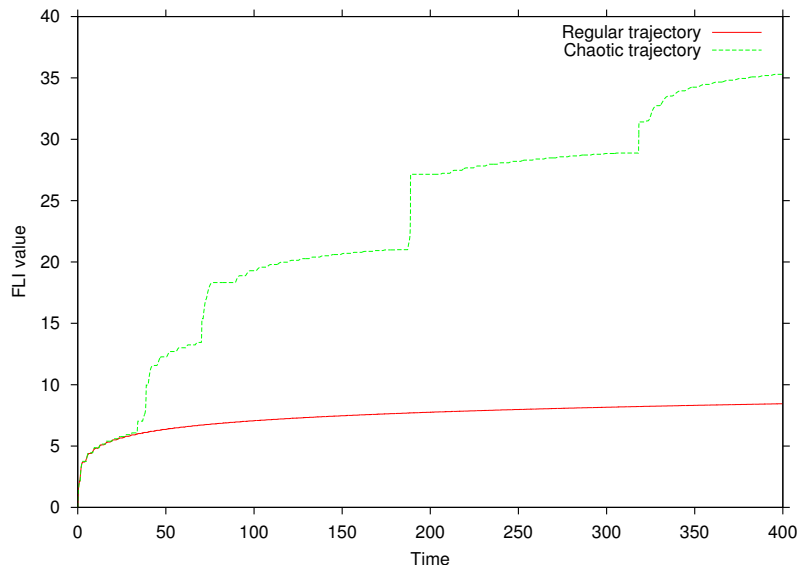


**Figure 5: Variation of the FLI value with time for two different trajectories in the PCR3BP corresponding to the Europa-Jupiter system at  $C = 3.0$ . The solid curves correspond to a regular trajectory ( $x = 0.9816$ ,  $y = 0.0$ ,  $\dot{x} = 0$ , at  $C = 3.0$  in the Jupiter-Europa system) while the dashed curves correspond to a chaotic trajectory ( $x = 0.981$ ,  $y = 0.0$ ,  $\dot{x} = -0.003$ ).**

This example shows us that the use of the FLI requires a preliminary calibration

---

\*\*That is the ratio  $(FLI(chaotic) - FLI(regular)) / FLI(regular)$

to determine the integration time span  $T$  considered as well as the minimum value of the FLI corresponding to a stable trajectory. The longer the time span  $T$  the more detail one can obtain for the dynamics, but also the larger the computational effort needs to be. For our purpose a value of less than one hundred of characteristic time of our system (here the orbital period of the primaries) seems sufficient. With these values the discrepancy in the FLI value between the regular and chaotic motion is of more than one order of magnitude.

Concerning the second calibration one can use the knowledge of a reference stable trajectory, for example in the case of a stability region around a periodic orbit where the FLI value of the reference periodic orbit can be used. More generally, we will see in the next subsection that the relative difference in the FLI value between sets of trajectories is in fact the real parameter of interest to us since it reflects the change in stability properties of the trajectories. This relative difference increases with the time span  $T$  used and should be considered in the setting of the first calibration.

## FLI Maps and Stability Regions

Given the above framework one can generate FLI maps in order to determine the stability domains in the region of phase space of interest by following the steps summarized below:

- Parameterize the region of phase space of interest.
- Sample the corresponding parameter space in order to generate initial conditions.
- Propagate the chosen points to generate a value of the FLI with each initial condition over a given time span  $T$ .
- Generate the density plot of the computed FLI values over the parameter space.

For example, taking as the system and region of interest the system and Poincaré section considered in Figure 4, the parameter space is given as the  $(x, \dot{x})$ -space and the remaining initial conditions are given as  $y = 0$  and  $\dot{y} = \sqrt{2\Omega - C - \dot{x}}$  with  $C = 3.0$ . For a time span of  $T = 400$  the resulting FLI map, computed with a grid of  $400 \times 400$  points, is presented in Figure 6. As we can observe there is a sharp contrast between the stability region of densely filled invariant tori and the unstable region of chaotic trajectories which allows us to recover the features observed in Figure 4 with the only help of the FLI.

In order to better understand the meaning of the results provided by the FLI, we investigated in greater detail a small neighborhood of the stability region around  $x = 0.98207$  at  $\dot{x} = 0$  in the above example. While the theory and the comparison with a Poincaré map indicate that low values of the FLI would generally correspond

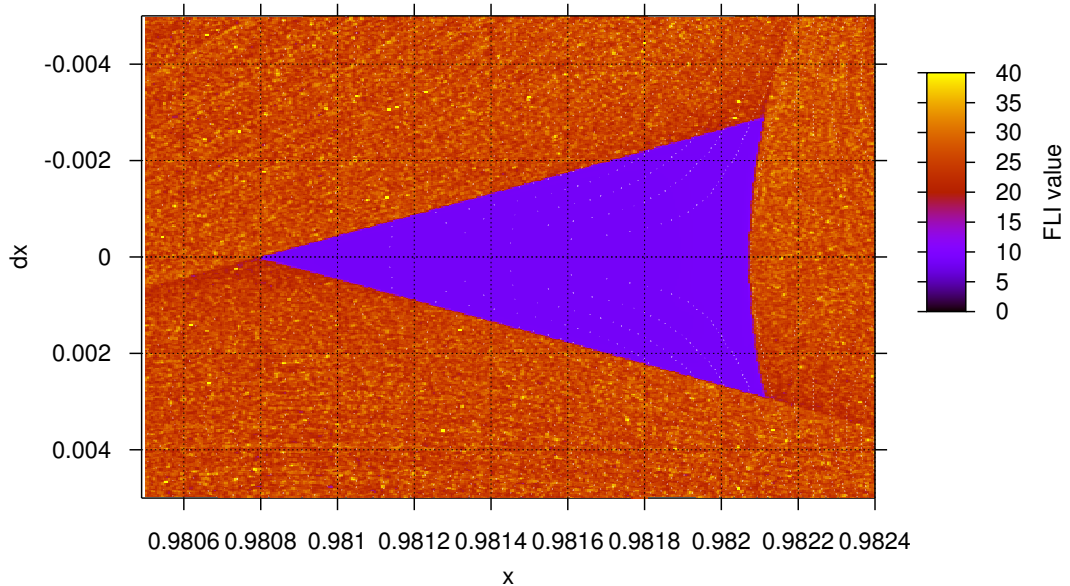


**Figure 6: FLI map corresponding to the Poincaré map presented in Figure 4.**

to stable motion, these results are so far only qualitative and a more quantitative investigation seems desirable.

Figure 7 presents the value of the FLI computed on a fine grid around the chosen boundary, which indicates that the contrast on the Poincaré map is the result of a large jump of the FLI value over a very small scale, of order less than  $10^{-9}$ . For  $x = 0.98207361456$ , the FLI value is  $\sim 23$ , while for  $x = 0.9207361458$  the FLI value is  $\sim 40$ . Figure 8 presents the plots of the path of the corresponding trajectories for a time span of  $T = 40000$ . It is observed that the trajectory with a low FLI value does indeed remains stable (small bounded variation from the nominal DRO) while the trajectory corresponding to a large FLI value shows a large variation in its path, moving from a domain dominated by Jupiter's gravitational field to a region dominated by Europa's gravity field.

Thus, we observe that while the computation of the FLI is only an estimation of the regularity properties of trajectories and that stability regions are only approximated by regions dominated by regular motion, the results provided at the energy values considered are rather sharp.

To conclude this section, we remark that because of the strong variations in the dynamical behavior observed at the boundary of the stability region considered the short time numerical integration (on a length scale on the same order as that con-

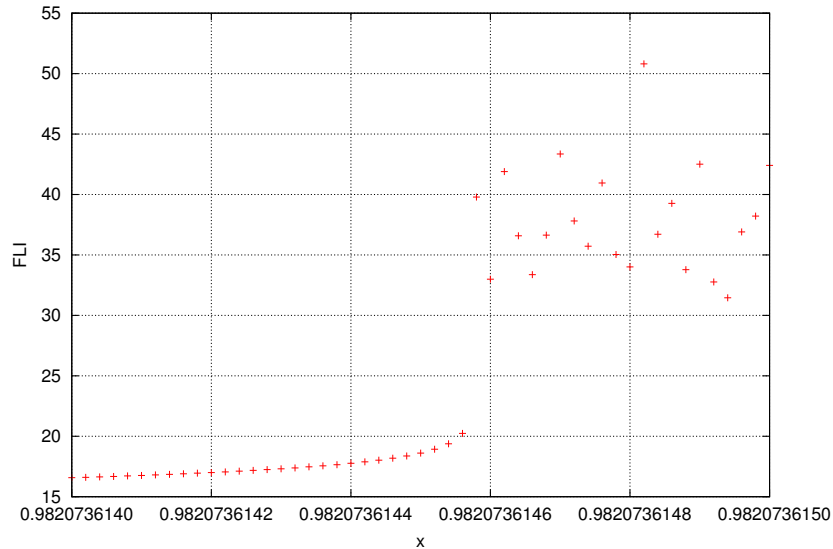


**Figure 7: Zoom of the FLI values near the boundary of the stability region.**

sidered for the above FLI computations  $T = 400$ ) of the trajectories alone (without integrating the tangent vector along the trajectory) should give a good approximation of the stability region. The stability could be checked for example, by assuming a trajectory to be unstable if it moves an arbitrary distance away from the DRO. The precise criterion to use seems rather arbitrary and would in that case come from a more experimental standpoint. Such computations would not a priori indicate any long term stability results.

On the contrary, the FLI provides us with a definite method to characterize the stability properties of trajectories via a single, easily computable scalar. Moreover, we have seen that the FLI has some strong theoretical foundations that give confidence in the long term stability properties. While these foundations are still unrigorous, in the sense that the FLI value has not been quantitatively related to the diffusion time of the trajectories (a relation which should also include the grid size used), the numerical results obtained with a simple calibration seem sufficient to obtain a good estimate of the extent of long term stability regions. Because of this missing step (and for the sake of validating the results obtained), the final trajectory chosen in the course of a design process should be integrated over the desired length of time to guarantee the required stability properties.

From a computational viewpoint the evaluation of the FLI, which requires the integration of a tangent vector, is a little more costly than the computation of the trajectory alone (though the cost of the condition used for deciding upon the stability property of the trajectory may well be more expensive than the computation of the FLI). Thus, while the generation of short time integration stability maps (without

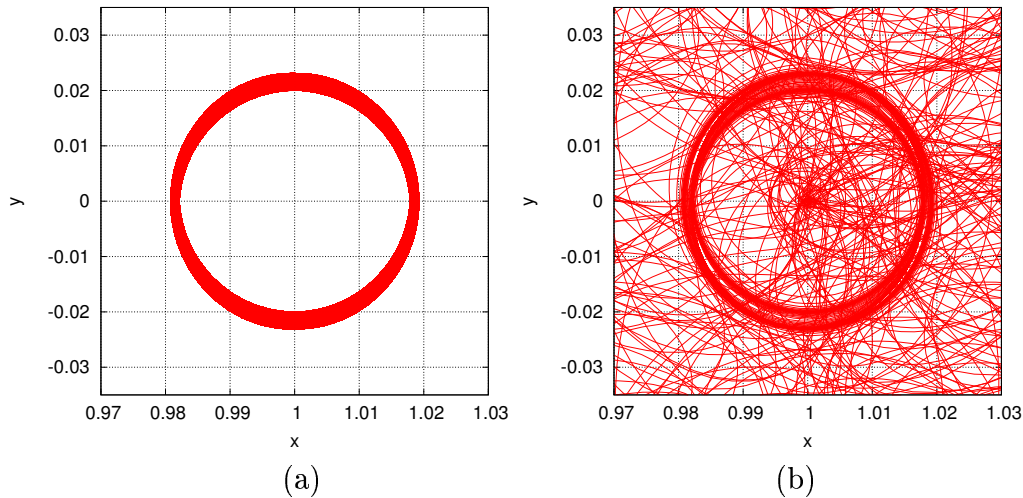


**Figure 8: Two trajectories at the boundary of the stability region associated with a DRO in the PCR3BP ( $\mu = 2.528 \times 10^{-5}$ ). The integration time is  $T=40000$  and the initial condition are given by  $y = \dot{x} = 0$ ,  $C = 3.0$  and  $x = 0.98207361456$  (a),  $x=0.98207361458$  (b).**

the use of the FLI) may well be sufficient for some problems, we think that the information brought by the FLI out-weighs the small computational effort overhead associated with it.

## APPLICATIONS AND DISCUSSION

In this last section we present some results obtained about the stability regions around the DROs in the circular restricted three body problem. These results allow us to illustrate some of the strengths of using an indicator as opposed to a Poincaré map, as well as indicate some directions for future research.

### Variation with $C$

We have seen that the stable regions can be approximated by a set of trajectories corresponding to low values of the FLI while the boundary of such regions is characterized by a large jump in the FLI value, the precise value of which are determined by the preliminary calibration. Thus, in order to minimize the computational effort to characterize the stability regions, one can simply set a threshold value for the FLI in the value gap at the boundary, say  $FLI_{threshold}$ , and track the level curve for this value. The resulting curve is an approximation of the stability region boundary.

The tracking process can be achieved by using a similar algorithm as the one presented in reference (Ref. 18). The core of the algorithm consists of a dichotomy

process to improve the accuracy over a bracketing pair of the desired level curve. That is, assuming given two initial conditions on the Poincaré section considered in the previous example,  $X_1 = (x_1, \dot{x}_1)$  and  $X_2 = (x_2, \dot{x}_2)$  with FLI values  $FLI_1$  and  $FLI_2$  such that  $FLI_1 < FLI_{threshold} < FLI_2$ , then one can compute the mid point of the segment joining  $X_1$  and  $X_2$  and compute the corresponding FLI value,  $FLI_{mid}$ . If  $FLI_{mid} > FLI_{threshold}$ , then the boundary of the stability region will lie between  $X_1$  and  $X_{mid}$ . Similarly, if  $FLI_{mid} < FLI_{threshold}$ , the process can be continued between  $X_{min}$  and  $X_2$  until the distance between the two end points of the bracketing pair is small enough. The initial bracketing pair is obtained by starting from a known stable point, such as the nominal DRO at the energy considered, and moving outwardly along a ray in the Poincaré section considered and emanating from this point (“step-walk” process). When a point with an FLI value larger than the threshold value has been found an initial bracketing pair has been obtained. Finally, the last item in this algorithm consists of obtaining a neighborhood bracketing pair once a corrected pair has been obtained. This can be done by rotating the given pair about the nominal initial point and locally adjusting the interval by a step-walk process similar to the initialization phase.

The advantage of using a boundary algorithm lies in the fact that the computational effort is lowered compared to using a full grid, as was used in Figure 6. For each value of  $C$  one thus obtains a curve representing the boundary of the stability region and the variation of  $C$  allows us to represent the stability region as a tubular surface. Figure 9 shows the results of such computations.

We note that as the DRO family crosses the libration point regions the size of the stability regions shrink until vanishing completely at two bifurcation points with an unstable periodic orbit of period approximately 3 times the period of the DROs in these regions. These unstable periodic orbits represent the vertices of the triangular shaped stability region. We should like to note however, that these results have already been observed<sup>16</sup> using a Poincaré map, and thus support the validity of the method adopted.

## Spatial Problem

While the above computations have been restricted to the planar case, where Poincaré maps can be used to check the prediction obtained, one of the advantage of the FLI maps is that they are not restricted to planar problems (as opposed to Poincaré maps which are difficult to use in systems with more than two degrees of freedom). For example, Figures 10-12 present two dimensional slices of the stability region around a DRO in the spatial, circular restricted three body problem. As we can observe, while the stability region does extend in the out-of-plane direction it remains rather confined to small inclinations. The dynamics around the boundary of this spatial stability region is however more complex than in the planar case and small

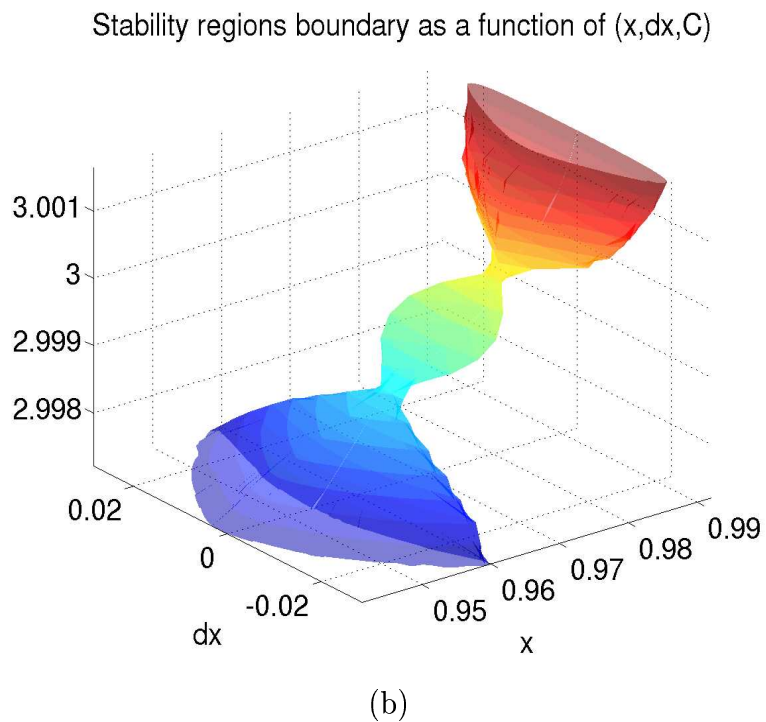
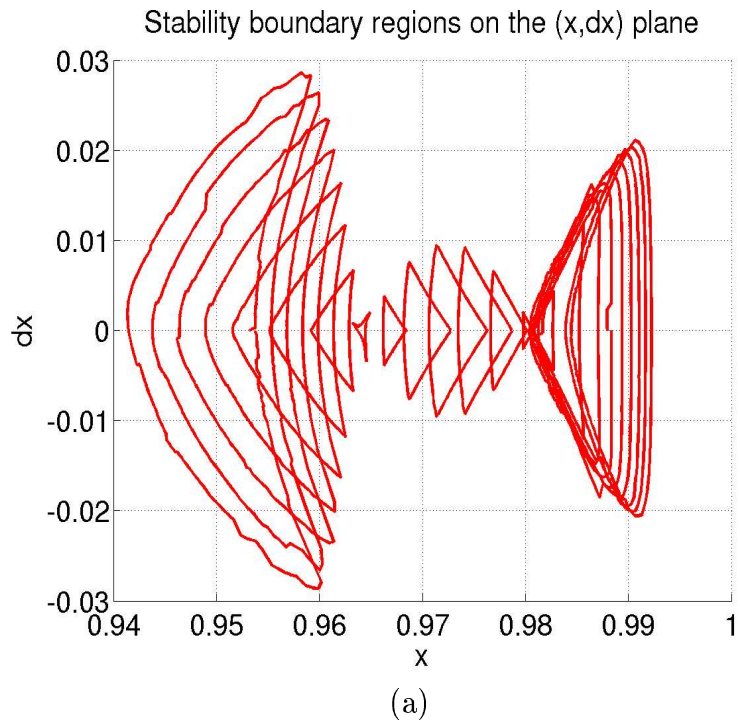


**Figure 9: Boundaries of the stability region associated with DROs in the Europa-Jupiter PCR3BP as a function of  $C$ : (a) projection on the  $(x, \dot{x})$ -plane; (b) three dimensional representation.**

disconnected stability regions seem to exist apart from the main stability region.

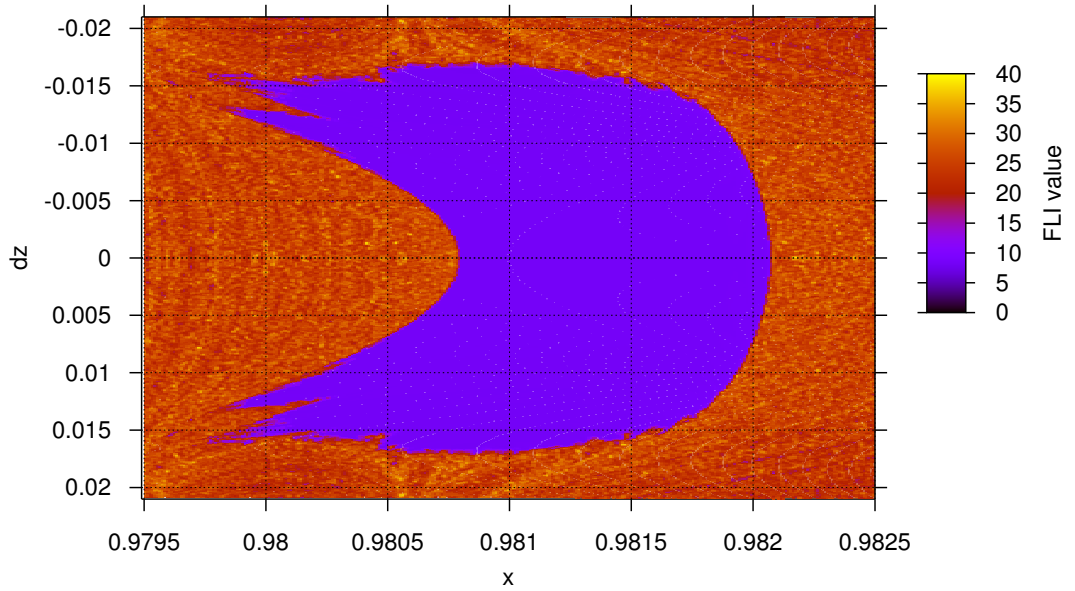


**Figure 10:** Section of the stability region when  $x$  and  $\dot{z}$  are varied for  $y = 0$ ,  $z = 0$  and  $C = 3.0$  in the Europa-Jupiter system.

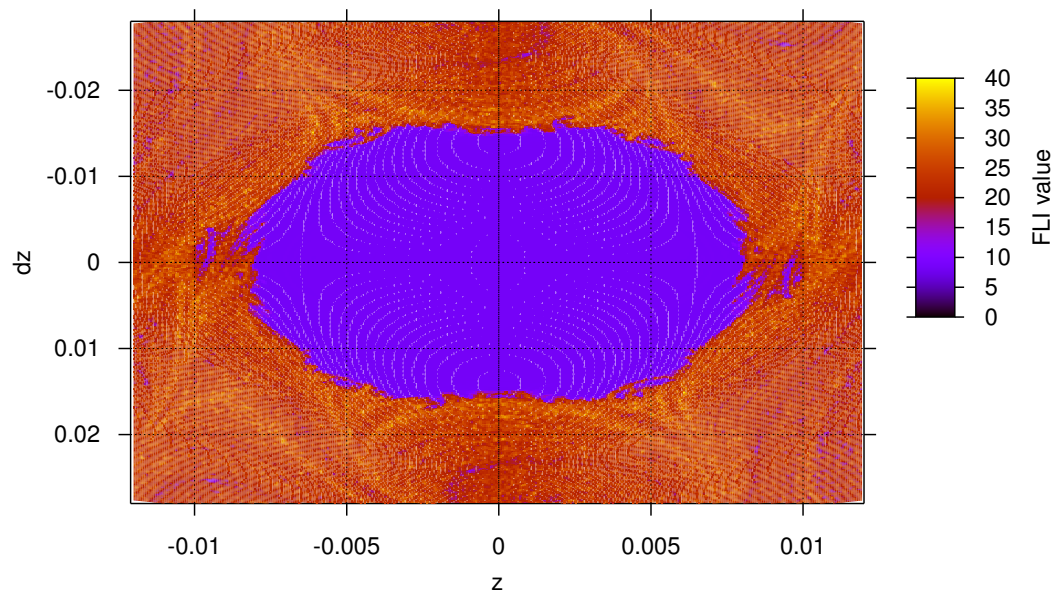


**Figure 11:** Section of the stability region when  $z$  and  $\dot{z}$  are varied for  $y = 0$ ,  $x = 0.9815$  and  $C = 3.0$  in the Europa-Jupiter system.

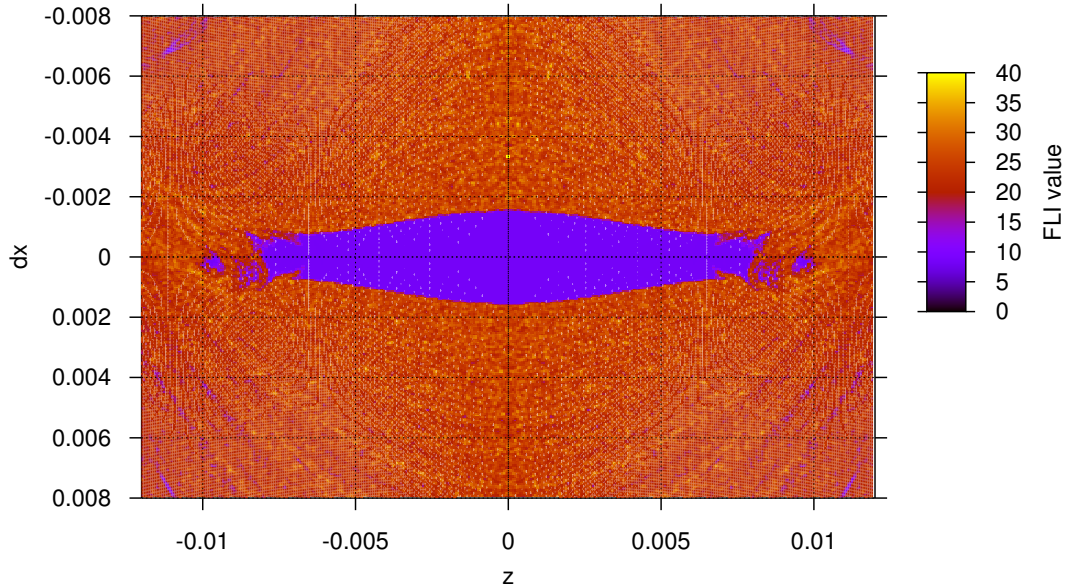


**Figure 12:** Section of the stability region when  $z$  and  $\dot{x}$  are varied for  $y = 0$ ,  $x = 0.9815$  and  $C = 3.0$  in the Europa-Jupiter system.

In the same realm of ideas, we note that the use of the FLI is in fact not restricted to autonomous or conservative systems, and can a priori be used with an ephemeris model.

## CONCLUSION

This paper investigated the use of a chaoticity indicator, the Fast Lyapunov Indicator, in order to compute the extent of the stability regions that exists around the stable periodic orbits, such as the Distant Retrograde Orbits. The method has been found to predict very well the long term stability of trajectories while considering only a relatively short integration time span. As compared to the use of Poincaré maps, this method can be applied to any spatial and non-autonomous system, the stability property of the trajectories being simply represented by a single scalar.

It has been observed that a large jump in FLI value occurs at the boundary of the stability region around some DROs which allows us to compute the variation of such stability regions with respect to the Jacobi constant by only computing the boundary of the stability regions as a level curve of the FLI maps. This process can be viewed as a reduction of the dimension of the problem considered.

While only two dimensional, Cartesian slices of initial conditions have been considered in this paper, the theory behind the definition of the FLI indicates that further

reduction in the dimensionality of the data set characterizing the stability regions should be obtained by generating FLI maps over the action variables of the system, as was considered for a sample Hamiltonian system in references (Refs. 6, 8, 11). This reduction should result in a concise representation of the stability properties of the system and may help in using this information to design robust low thrust transfers. Future work should address such issues as well as the formal relationship between the grid size, integration time, and long term stability properties of the trajectories considered.

## ACKNOWLEDGEMENT

The research in this paper was sponsored by the Jet Propulsion laboratory, California Institute of Technology, under contract to the National Aeronautics and Space Administration. The bulk of the research was carried out when the first author was working as a post-doctoral scholar at the California Institute of Technology under the supervision of Dr. Martin W. Lo and Prof. Alan H. Barr.

## REFERENCES

1. Arnol'd, V.I., "Small Denominators and Problems of Stability of Motion in classical and Celestial Mechanics", *Russina Methematical Surveys*, Vol. 18, No. 9, 1963.
2. Deprit, A., Henrard, J., "Natural Families of Periodic Orbits", *The Astronomical Journal*, Vol. 72, No. 2, pp. 158-172, 1967.
3. Friedlander, A.L., "Jupiter Orbiter Lifetime - Hazard of Galilean Satellite Collision", *Journal of the Astronautical Sciences*, Vol. 23, No. 4, pp. 349-368, 1995.
4. Froeschle, C., Lega, E., Gonzi, R., "Fast Lyapunov Indicators. Application to Asteroidal Motion", *Celestial Mechanics and Dynamical Astronomy*, Vol. 67, pp 41-62, 1997.
5. Froeschle, C., Lega, E., "On the Structure of Symplectic Mappings. The Fast Lyapunov Indicator: A Very Sensitive Tool.", *Celestial Mechanics and Dynamical Astronomy*, Vol. 78, pp 167-195 2000.
6. Froeschle, C., Guzzo, M., Lega, E., "Graphical Evolution of the Arnold Web: From Order to Chaos", *Science*, Vol. 289, pp 2108-2110, 2000.
7. Gomez, G., Koon, W.S., Lo, M.W., Marsden, J.E., Masdemont, J., and Ross, S.D., "Invariant Manifolds, the Spatial Three-Body Problem and Space Mission Design", paper AAS 01-31 presented at the Astrodynamics Specialist Meeting, Quebec City, Canada, August 2001.
8. Guzzo, M., Lega, E., Froeschlé, C., "On the Numerical Detection of the Effective Stability of Chaotic Motions in Quasi-integrable Systems.", *Physica D*, Vol. 163, pp 1-25, 2002.

9. Hénon, M., "Numerical Exploration of the Restricted Problem. V: Hill's Case - Periodic Orbits and their Stability.", *Astronomy and Astrophysics*, Vol. 1, No. 2, pp. 223-238, 1969.
10. Laskar, J., "The Chaotic Motion of the Solar System: A Numerical Estimate of the Size of the Chaotic Zones.", *Icarus*, Vol. 88, pp.226., 1990.
11. Lega, E., Guzzo, M., Froeschlé, C., "Detection of Arnold diffusion in Hamiltonian Systems", *Physica D*, Vol. 182, pp 179-187, 2003.
12. Lyapunov, A.M., "Problème General de la Stabilité du Mouvement", *Annals of Mathematical Studies, Princeton University Press*, Vol. 17, 1949.
13. Morbidelli, A., *Modern Celestial Mechanics. Aspects of Solar System Dynamics*, Advances in Astronomy and Astrophysics, Taylor and Francis, 2002.
14. Oseledec, V.I., "A Multiplicative Ergodic Theroem. The Lyapunov Characteristic Numbers of Dynamical Systems", *Moscow Mathematical Society*, Vol. 19, pp. 197-231, 1968.
15. Perry, A.D., Wiggins, S., "KAM Tori are Very Sticky - Rigorous lower bounds on the time to move away from an invariant Lagrangian torus with linear flow", *Physica D*, Vol. 71, No. 1-2, pp. 102-121, 1994.
16. Simó, C., Stuchi, T.J., "Central Stable/Unstable Manifolds and the Destruction of KAM Tori in the Planar Hill Problem.", *Physica D*, Vol. 140, 2000.
17. Szebehely, V., *Theory of Orbits*, Academic Press, New York, 1967.
18. Villac, B.F., Scheeres, D.J., "A Simple Algorithm to Compute the Hyperbolic Invariant Manifolds near  $L_1$  and  $L_2$ ", Paper AAS 04-243, presented at the Space Flight Mechanics Meeting, Maui, Hawaii, February 2004.